Effect of Gravity and Noncondensable Gas Levels on Condensation in Variable Conductance Heat Pipe

Yasunori Kobayashi,* Akira Okumura,† and Toshihisa Matsue†
Institute of Engineering Mechanics, University of Tsukuba, Tsukuba, Ibaraki 305, Japan

An experimental and analytical study was conducted to examine the flowfield behavior of a vapor-noncondensable gas mixture and its effect on heat transfer rate in the condenser of a variable conductance heat pipe (VCHP) or thermosyphon. Detailed temperature distributions and heat transfer rate were measured, and a flowfield visualization was made using a laser holographic interferometer. In order to investigate the dominant physical parameters in the flowfield, a numerical simulation was performed. It was found that the gravity force and levels of noncondensable gas contained have a strong effect on the location and the profile of an interfacial layer. The proposal of the formation of a clear diffusion front layer in the condenser would lead to an erroneous interpretation of thermofluid dynamic behavior of VCHPs for terrestrial use or ground-based testing.

Nomenclature

a = value of c_v or $\ell_n m$
c = molar density, kg/mole
D_{VG} = binary diffusion coefficient, m^2/s
F = constant appearing in Eq. (11)
Gr_C = Grashoff number for density gradient $[=g\zeta(a-\bar{a})L^3/\nu^2]$
Gr_T = Grashoff number for temperature gradient $[=g\beta(T-\bar{T})L^3/\nu^2]$
g = acceleration of gravity, m/s^2
h = mesh size in numerical scheme
k = thermal conductivity, W/mK
L = width of condenser channel, m
Mi = molecular weight of i species, kg/mole
m = molar weight of mixture $(=\chi_V M_V + \chi_G M_G)$, kg/mole
n = coordinate x or y perpendicular to wall boundary
n_G = mole of noncondensable gas given initially, kg/mole
Pe = Peclet number $(RePr)$
Pr = Prandtl number $(=\alpha/\nu)$
R = constant representing Re, $PrRe$, or $ScRe$ in Eq. (11)
Re = Reynolds number $(=u_0 L/\nu)$
Sc = Schmidt number $(=\alpha/D_{VG})$
T = temperature, K
U,V = dimensionless mass average velocities
u,v = dimensional mass average velocities, m/s
V_{0L} = volume of flowfield in the condenser, m^3
w = liquid velocity in the thin film layer, m/s
X_E, = dimensionless length of active cold wall (B-V in Fig. 2)
X,Y = dimensionless positions
x,y = dimensional positions, m
α = thermal diffusivity, m^2/s
β = coefficient of density gradient for temperature $-\left(\frac{1}{\rho}\frac{\partial\rho}{\partial T}\right)$
δ = thickness of liquid film on the cold plate, m
ζ = coefficient of density gradient for concentration $-\left(\frac{1}{\rho}\frac{\partial\rho}{\partial a}\right)$
Θ = dimensionless temperature
θ = angle of the model inclined from vertical, deg
Λ = dimensionless expression of $\ell_n m$
μ = coefficient of viscosity, $Pa \cdot s$
ν = kinetic viscosity, m^2/s
ξ,η = coordinate systems in the liquid film, m
ρ = density, kg/m^3
Φ = variable representing C_V, Λ, Θ, Ω, or Ψ
χ = mole fraction
ψ,φ = stream function
Ω,ω = vorticity

Subscripts
G = noncondensable gas
L = working liquid
V = working fluid, vapor
W = wall, boundary
0 = inlet section of the condenser
$\bar{}$ = averaged or reference value

Introduction

THE behavior of vapor flow in the condenser region of a variable conductance heat pipe (VCHP) has been investigated as one of the most interesting thermofluid dynamic phenomena for two reasons. The first reason is that it has stimulated academic interest in its characteristic convective motion, combined with the binary diffusion between the vapor and noncondensable gas, which is strongly coupled with vapor condensation on the surrounding wall. Appearance of the interfacial layer in the condenser, which is known to divide the flowfield into two regions, e.g., a region of pure vapor and that of noncondensable gas mixed with saturated vapor, is also an essential phenomenon in the flowfield in the VCHP. The second reason is based on a practical need for the development of a high-efficiency heat transfer device with temperature regulation capability.

Work in this field was pioneered by T. P. Cotter[1] in 1965, and subsequent studies on the flowfield in the heat pipe were developed during the 1960s.[2,3] Rohani and Tien[4] were the first to propose an elaborate numerical model for the flowfield behavior, which was followed by many investigators for better analytical modeling and detailed experiment.[5-8] Recent exper-

Presented as Paper 89-1747 at the AIAA 24th Thermophysics Conference, Buffalo, NY, June 12-14, 1989; received July 4, 1989; revision received and accepted for publication Nov. 17, 1989.

*Professor, Institute of Engineering Mechanics. Member AIAA.
†Graduate Student, Graduate School of Engineering.

imental investigations[9,10] of such a flowfield revealed some of the significant thermofluid dynamic features and instabilities which are associated with phase changes in the working fluid. According to Ref. 9, the temperature and pressure never remain stable but fluctuate fairly intermittently and/or randomly even in its steady-state thermal condition. This occurs regardless of the amount of noncondensable gas constituents or the heat load applied to the heat pipe. The phenomenon is apparently driven by the coupling effect of a vapor pressure fluctuation related to a phase change of the fluid, featuring the flowfield in an enclosure, such as heat pipes. In addition, the effect of the gravity and the levels of molecular weight ratio on the interfacial layer in the flowfield were also examined in Ref. 9.

A complete analytical formulation of the randomly fluctuating flowfield by employing phenomenological equations would be almost impossible without detailed information on the phase-change mechanism requiring a microscopic description of vapor and gas molecules. However, it has been confirmed by experiment and by empirical analyses that the average values of temperature and pressure in the flowfield are sufficient to calculate an averaged heat transfer rate or heat-pipe performance. Therefore, even in recent analytical investigations,[11-13] only average values of flowfield have been evaluated although more rigorous boundary conditions are introduced for physical properties of mass, energy, and phase equilibrium and are incorporated into the effect of the gravity force and the levels of molecular weight ratio on the flowfield.

The main objective in this study is to investigate a vapor flowfield in the condenser of the VCHP or the thermosyphon and to measure the effect of gravity force on the flowfield with respect to different vapor-noncondensable gas molar ratios. The study includes a detailed experimental survey of the flowfield in a two-dimensional condenser region and a simulation analysis of the flowfield employing a suitable mathematical condensation model and flowfield boundary conditions. It should be noted that, in order to formulate the phenomena in terms of mass average velocities u,v rather than mole-average velocities, a different type of mass concentration, namely the logarithm of the mean molecular weight of the mixture $\ell n\ m$ is introduced. This was first suggested by C. H. Bedingfield Jr. and T. B. Drew[14] as being a more realistic formula for gaseous diffusion phenomena such as those used in our experiment. The difference in numerical results between this new variable $\ell n\ m$ and molar concentration C_V incorporated into binary-diffusion equation is also discussed.

Experimental Setup and Method

The experimental setup and layout used are essentially the same as those described in Ref. 9 except that a new test apparatus was fabricated in order to measure the detailed temperature distributions in the flowfield. A schematic drawing of the apparatus representing the VCHP or the thermosyphon condenser is shown in Fig. 1a. The body of the apparatus is made of brass and has a rectangular, cross-sectional area of 18 mm in width by 50 mm in depth and 185 mm in internal length. A pair of optical windows were installed as side walls for flow visualization, and one copper wall, which was actually a flat, hollow cavity box of 130 mm in length and 5 mm in thickness, fixed on the body wall, was cooled by circulating water through its cavity.

The other walls were covered with 5-mm-thick Teflon plates to maintain the wall surfaces adiabatic. The purpose of this is to distinguish the effect of wall temperature differences on vapor flows in the condenser as well as to obtain an accurate heat transfer rate at the cold plate. A two-dimensional flowfield is approximated in the condenser in the preliminary experiment. In addition, no wick structure is provided in the condenser in order to elucidate the fluid dynamic phenomena of vapor condensation on the cold plate and therefore to eliminate a possible vapor-wick interaction, which would complicate the flowfield analysis at that point.

A total of 35 copper-constantan thermocouples having 0.2 mm (2×10^{-4} m) diam were installed inside the apparatus in six groups, A to F for convenience, through four ports as shown in Fig. 1b. These thermocouples remained in position without support, except those of C-group, which were buried in the limb of the copper plate through its back by drilling small holes. The evaporator section of the apparatus is a simple structure consisting of a brass tube having a 30-mm diam and a 300-mm length. It is attached to the condenser-end flange, and a Teflon plate was inserted to minimize the heat conduction between the two sections. Heat energy was supplied to the evaporator end through an electric heater.

Our previous studies of the flowfield visualization for different combinations of vapor-gas mixtures confirmed that in the

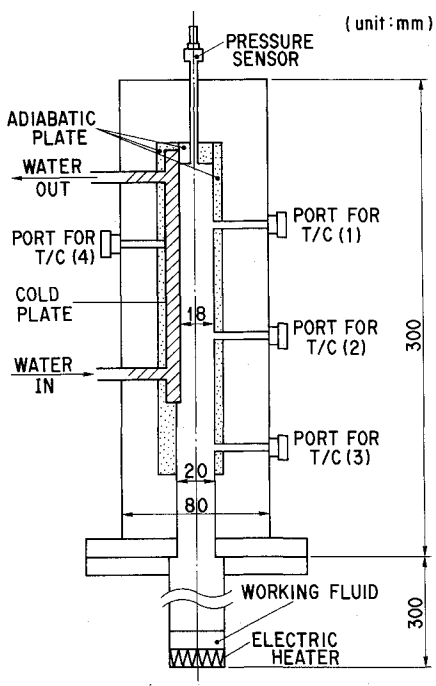

Fig. 1a Rough sketch of test apparatus for VCHP or thermosyphon condenser.

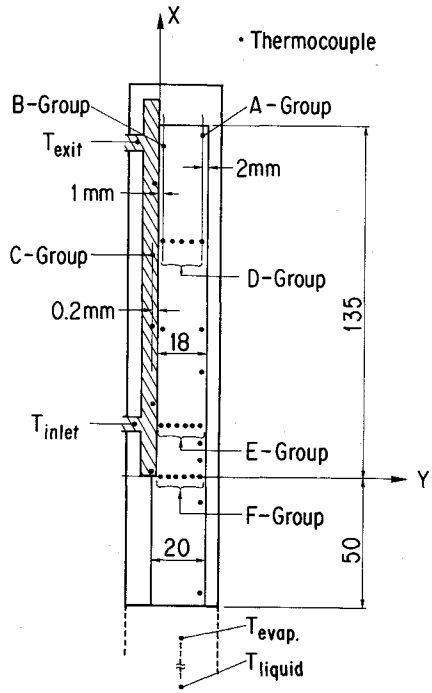

Fig. 1b Locations of 35 thermocouples installed in the condenser section.

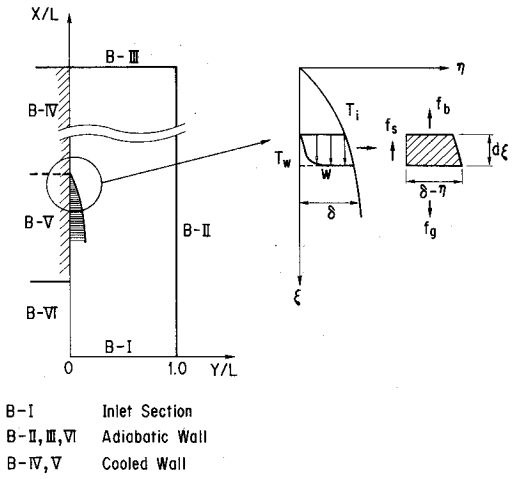

Fig. 2 Schematics of analytical flowfield boundaries and coordinate system used for discussion of liquid film at B-V.

case where M_V is much smaller than M_G ($M_V < M_G$), e.g., with a water-argon mixture, the flowfield becomes unstable, and no clear interfacial layer appears; whereas in the reverse case ($M_V > M_G$) such as a benzene-helium mixture, we observed a clear interfacial layer indicating a finite region with a sharp density gradient. In this paper, the numerical results of the benzene-air mixture are discussed. (Discussions for the other cases are included in Ref. 7.) Measurements were made maintaining a large temperature difference between the vapor and the cold plate (up to 50°C) in order to distinguish the condensing vapor flow at the wall.

The effect of gravity on the vapor flows—especially on the formation of the vapor-gas interfacial layer, was investigated by holding the apparatus both in a vertical and an almost horizontal (88 deg inclined from vertical direction) position. The configuration in the former position is referred to as the "vertical condenser" and the latter, the "near-horizontal condenser" hereafter. In the near-horizontal position, two conditions of the cold plate were examined, i.e., facing downwards (as a ceiling wall) and upwards (floor wall). Temperature data were acquired by scanning the 35 thermocouples over a 12-s period. Static pressure in the flowfield was monitored by the pressure transducer located at the top of the apparatus (see Fig. 1a).

Heat transfer rates in the condenser were calculated from the flow rate and the temperature difference between the inlet and the outlet of a water circulation tube and also from the electric power applied to the evaporator wall. After compensating for any heat loss from the exterior surface of the apparatus to ambient temperature by radiation and convection, it was found that both sets of data agreed within an accuracy of 7%. Consequently, the heat transfer rates obtained from an electric power input have been incorporated into this paper.

Vapor flowfields in the condenser with different molar concentration of noncondensable gas constituents were visualized by means of real-time laser holographic interferometry. The fringe patterns on the laser holographic interferograms were analyzed to obtain quantitative temperature and density distributions in the flowfield with the aid of reference temperature taken by the thermocouple positioned at the adiabatic region.

Analysis

Governing Equations

The flowfield considered here is a double-diffusive, forced, convection flow, affected by the buoyancy force of both the temperature and density differences. The analytical flowfield is assumed to have a rectangular shape with six boundaries in order to compare them with those used in the experimental apparatus, as shown in Fig. 2. The boundary B-I in the figure represents the inlet section of the condenser and that of B-IV and B-V represent the cold plate, and the remainder are adiabatic walls. The boundary B-V is acting as a molecular sink for the vapor flow but as an impermeable wall for the noncondensable gas. However, B-IV is a cold, impermeable wall both for vapor and noncondensable gas with no condensation involved.

Three sets of conservation equations for a fluid mixture and for the conservation of species or binary-diffusive transport equation have been incorporated. In the latter, two variables are considered: the molar concentration c_V under a constant density and the mean molecular weight of a mixture m in the form of $\ell n\, m$ under a constant concentration. If uniform pressure is assumed in the flowfield as described below, it is apparent that the constant concentrations should be applied near the interfacial layer for logical consistency of the analysis.

The following assumptions are made:

1) The entire flowfield is two dimensional under a steady state and has a uniform pressure field determined by the saturated vapor temperature at the inlet of the condenser (B-I).

2) Both the vapor and the noncondensable gas are incompressible and ideal gases.

3) All the physical properties are constant evaluated at the average temperature between the inlet and the cold wall sections.

4) Poiseuille vapor flow is assumed at the inlet (B-I).

5) A thin liquid film is formed on the condensing wall (B-V) where a phase equilibrium is maintained with a constant heat flux on the interface. The film thickness is ignored in the calculation.

Equations are summarized below making the assumptions mentioned above:

Continuity equation of mixture

$$\frac{\partial u}{\partial x}+\frac{\partial v}{\partial y}=0 \tag{1}$$

Momentum equation of mixture, under constant density condition

$$u\frac{\partial u}{\partial x}+v\frac{\partial u}{\partial y}=\nu\left(\frac{\partial^2 u}{\partial x^2}+\frac{\partial^2 u}{\partial y^2}\right) + g\zeta\cos\theta(a-\bar{a})+g\beta\cos\theta(T-\bar{T}) \tag{2}$$

$$u\frac{\partial v}{\partial x}+v\frac{\partial v}{\partial y}=\nu\left(\frac{\partial^2 v}{\partial x^2}+\frac{\partial^2 v}{\partial y^2}\right) + g\zeta\sin\theta(a-\bar{a})+g\beta\sin\theta(T-\bar{T}) \tag{3}$$

Energy conservation of mixture, neglecting source term by the external force

$$u\frac{\partial T}{\partial x}+v\frac{\partial T}{\partial y}=\alpha\left(\frac{\partial^2 T}{\partial x^2}+\frac{\partial^2 T}{\partial y^2}\right) \tag{4}$$

where the second and third terms of the right side of Eqs. (2) and (3) represent the buoyancy force generated by concentration and temperature differences, respectively. The source term in the energy equation is ignored as it is negligible in this case.

The equation of binary diffusion is expressed in two ways depending on the condition assumed near the interfacial layer: For constant density

$$u\frac{\partial c_V}{\partial x}+v\frac{\partial c_V}{\partial y}=D_{VG}\left(\frac{\partial^2 c_V}{\partial x^2}+\frac{\partial^2 c_V}{\partial y^2}\right) \tag{5}$$

for constant concentration

$$u\frac{\partial \ell n\,\bar{m}}{\partial x}+v\frac{\partial \ell n\,\bar{m}}{\partial y}=D_{VG}\left(\frac{\partial^2 \ell n\,\bar{m}}{\partial x^2}+\frac{\partial^2 \ell n\,\bar{m}}{\partial y^2}\right) \tag{6}$$

where

$$\bar{m}=m/M_V$$

represents an average molecular weight of the mixture normalized by a vapor molecular weight, and u,v are mass average velocity components. The value of θ represents an attitude angle of the apparatus inclined from a vertical position ($\theta=0$). Introduction of a stream function together with the vortex equation allows us to rearrange the equations after nondimensionalization as follows:

$$\frac{\partial}{\partial X}\left(\frac{1}{Re}\frac{\partial \Omega}{\partial X}-U\Omega\right)+\frac{\partial}{\partial Y}\left(\frac{1}{Re}\frac{\partial \Omega}{\partial Y}-V\Omega\right)$$
$$+Gr_c\left(\sin\theta\frac{\partial A}{\partial X}-\cos\theta\frac{\partial A}{\partial Y}\right)+Gr_T\left(\sin\theta\frac{\partial \Theta}{\partial X}-\cos\theta\frac{\partial \Theta}{\partial Y}\right) \tag{7}$$

$$\frac{\partial}{\partial X}\left(\frac{1}{RePr}\frac{\partial \Theta}{\partial X}-U\Theta\right)+\frac{\partial}{\partial Y}\left(\frac{1}{RePr}\frac{\partial \Theta}{\partial Y}-V\Theta\right)=0 \tag{8}$$

$$\frac{\partial}{\partial X}\left(\frac{1}{ScRe}\frac{\partial A}{\partial X}-UA\right)+\frac{\partial}{\partial Y}\left(\frac{1}{ScRe}\frac{\partial A}{\partial Y}-VA\right)=0 \tag{9}$$

$$\left(\frac{\partial^2 \psi}{\partial X^2}+\frac{\partial^2 \psi}{\partial Y^2}\right)+\Omega=0, \qquad U=\frac{\partial \psi}{\partial Y}, \qquad V=-\frac{\partial \psi}{\partial X} \tag{10}$$

where A represents either Λ or C_V, and those physical properties of u_0, L, M_V, T_0, and T_W are used as references in the process of nondimensionalization as

$$X=\frac{x}{L}, \quad Y=\frac{y}{L}, \quad U=\frac{u}{u_0}, \quad V=\frac{v}{u_0}$$

$$\Psi=\frac{\varphi}{u_0 L}, \qquad \Omega=\frac{\omega L}{u_0}, \qquad \Theta=\frac{(T-T_W)}{(T_0-T_W)}$$

$$C_V=\frac{c_V-c_{V,W}}{c_0-c_{V,W}}, \qquad C_{V,W}=\frac{c_{V,W}}{c_0-c_{V,W}}, \qquad \Lambda=\frac{\ell n(m/m_W)}{\ell n(M/m_W)}$$

$$N=\frac{m-m_V}{M_V-m_W}, \qquad N_W=\frac{m_W}{M-m_W}$$

Numerical Calculation

Equations (7–9) have a common mathematical form expressed as

$$\frac{\partial}{\partial X}\left(\frac{1}{R}\frac{\partial \Phi}{\partial X}-U\Phi\right)+\frac{\partial}{\partial Y}\left(\frac{1}{R}\frac{\partial \Phi}{\partial Y}-V\Phi\right)+F=0 \tag{11}$$

where Φ represents A, Ω, or Θ, and R represents the constants Re, $PrRe$, or $ScRe$ in Eq. (7), (8), or (9), respectively. The value of F represents the last two terms in Eq. (7) or zero for Eqs. (8) and (9). Therefore, the calculation method and the coding process of the equations in finite-difference formulas are simplified. A method of centered difference scheme is applied for dissipation terms, and a second-order upwind differencing scheme is used for convection terms. In the calculation, the successive overrelaxation (SOR) method is employed. A general form of a finite-difference equation at grid points (i,j) employed in the calculation is written as

$$a_{i,j}\Phi_{i-1,j}+b_{i,j}\Phi_{i+1,j}+C_{i,j}\Phi_{i,j-1}$$
$$+d_{i,j}\Phi_{i,j+1}+e_{i,j}\Phi_{i,j}+F_{i,j}=0 \tag{12}$$

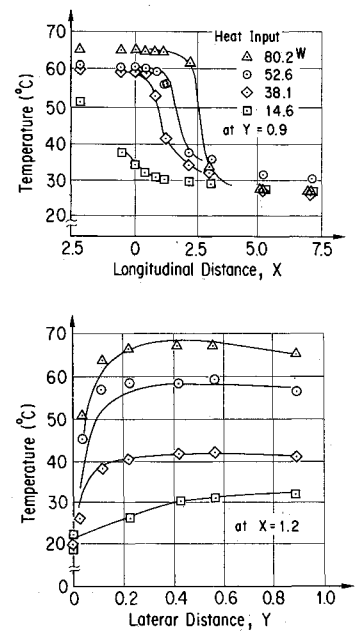

Fig. 3 Comparison of temperature distributions along and perpendicular to flow axis in the vertical condenser with respect to heat-load change ($n_G=0.002$ mole).

Giving the three dependent variables Ω, Θ, and A proper boundary conditions in order to make them converge simultaneously at the six flowfield boundaries produces a difficult and laborious calculation. After several conditions were examined, the following are examined in the current calculation. B-I: inlet section of the condenser where the incoming vapor flow is assumed to have a Poiseuille flow profile

$$\psi=Y^2(3-2Y), \qquad \Omega=6(2Y-1), \qquad C_v=\Theta=1$$

B-II, B-III, B-VI: adiabatic walls where Ω has a boundary value of a second-order accuracy Ω_W and the gradients of A and Θ perpendicular to the wall are zero

$$\frac{\partial A}{\partial n}=\frac{\partial \Theta}{\partial n}=0, \qquad \Omega=\Omega_w, \qquad \psi=0 \text{ (at B-II, B-III)}$$
$$\psi=1 \text{ (at B-VI)}$$

where Ω_W is given as (the Woods condition)

$$\Omega_W=-\tfrac{1}{2}\Omega_{W-1}-(3/h^2)(\psi_{W+1}-\psi_W) \tag{13}$$

B-IV: cold plate (inactive condensing wall) where no condensation takes place by the saturated vapor since its temperature is equal to that of the cold plate

$$A=\Theta=\psi=0, \qquad \Omega=\Omega_W$$

B-V: cold plate (active condensing wall) where the thickness of the film is very small, i.e., has a magnitude in the order of 10^{-4} m, which is less than in the present calculation. From the energy balance at this interface where $V_{G,W}=0$ and assuming an ideal gas, we obtain

$$V_{V,W}=\frac{(\Theta+\Theta_W)(1+N_W)}{X_E(1+\Theta_W)(N+N_W)} \tag{14}$$

In addition, assuming that the Clausius-Clapeyron relation holds between the liquid film and the saturated vapor, the expression for the temperature distribution on the liquid film

surface is formulated in terms of a function of temperature only. The final form of these equations after nondimensionalization are as

$$N=\frac{\chi-\chi_W}{1-\chi_W},\qquad C_V=(1+C_{V,W})\left(\frac{1+\Theta_W}{\Theta+\Theta_W}\right)\chi-C_{V,W}$$

$$\chi=\exp\left[T^*\frac{\Theta-1}{\Theta+\Theta_W}\right],\qquad T^*=-\Theta_W\ell n\,\chi_W,$$

$$\chi_W=\left(\frac{C_{V,W}}{1+C_{V,W}}\right)\left(\frac{\Theta_W}{1+\Theta_W}\right) \tag{15}$$

Next, momentum balance is considered at the interface (see Fig. 3b). When we assume that the wall temperature T_W is constant and the film surface temperature T_i varies with ξ, three forces, i.e., shear stress f_s, vapor buoyancy force f_b, and gravity force f_g, are balanced as shown:

$$\rho_L g(\delta-\eta)\mathrm{d}\xi=\mu_L\frac{\mathrm{d}w}{\mathrm{d}\eta}\,\mathrm{d}\xi+\rho_V g(\delta-\eta)\mathrm{d}\xi \tag{16}$$

Increase in mass flow rate G of the falling liquid is related to the vapor condensation velocity $v_{V,W}$ and is incorporated into Eq. (16) as

$$\frac{\mathrm{d}G}{\mathrm{d}\xi}\,\mathrm{d}\xi=\frac{\mathrm{d}G}{\mathrm{d}\delta}\,\mathrm{d}\delta=\frac{\rho_L(\rho_L-\rho_V)g}{\mu_L}\,\delta^2\,\mathrm{d}\delta=\rho_V v_{V,W}\,\mathrm{d}\xi$$

$$=\frac{\rho_0 u_0 L}{x_E}\,\mathrm{d}\xi \tag{17}$$

Further, balancing the total energy between the incoming vapor flow and the amount of condensed liquid volume, and assuming a constant heat flux to the wall (B-V), we obtain the following relation:

$$\Theta=\left(\frac{X_E-X}{X_E}\right)^{1/3}$$

after simple algebraic manipulation of Eqs. (14) and (15) using the following relations

$$\xi=x_E-x,\qquad \frac{\delta}{\delta_0}=\left(\frac{x_E-x}{x_E}\right)^{1/3}$$

$$\frac{T-T_w}{\delta}=\frac{T_0-T_w}{\delta_0}=\frac{Q}{kS_E}$$

where Q, S_E, and δ_0 are for the transferred heat load, the area of B-V, and the film thickness at B-VI, respectively.

No explicit restriction is postulated for the noncondensable gas contained in the flowfield, but in the numerical algorithm, the initial molar concentration

$$\bar{C}_G=\frac{n_G}{V_{0L}(c_0-c_{V,W})} \tag{18}$$

is monitored as a reference to the termination of the calculation.

Process of Numerical Calculation

Actual calculations in the computer code were run using the following process:

1) determine parameters of C_G, Θ, Pr, Sc, Gr_C, Gr_T from given physical properties, flow conditions such as initial noncondensable gas constituent $\bar{C}_G$, applied heat load Q, position of the apparatus θ, etc., and calculate N_W, and $C_{V,W}$;

2) set an arbitrary value for X_E;

3) calculate a common flowfield (convection terms) associated with the constant coefficients, a, b, c, d, and e in Eq. (12);

4) calculate the temperature field Θ by adding the thermal diffusion term to the results obtained in process 3;

5) calculate the concentration field A by adding the mass diffusion term to the results obtained in process 3;

6) calculate the vortex field Ω by adding the vortex diffusion term to the results obtained in process 3;

7) calculate the stream function ψ and velocity field U, V using the relation of Eq. (10);

8) repeat processes 3–7 until the values of Θ, Ω A, and ψ converge simultaneously;

9) calculate C_G in the flowfield, set a new value for X_E if C_G does not reach $\bar{C}_G$ in Eq. (18), then go to process 2 to start a new calculation.

10) All of the iteration calculation will be terminated when

$$\frac{\max(\Phi_{\mathrm{NEW}}-\Phi_{\mathrm{OLD}})}{\max(\Phi_{\mathrm{NEW}})}\le\varepsilon(=10^{-4})$$

is satisfied. The FACOM M780 model (20 MFLOPS) was used, and typical CPU times for each run were about 10 to 15 min depending on the given condition. A typical number of grid points of the numerical flowfield employed in the calculation was 3171 (or 21 by 151).

Results and Discussion

Experiment

Figure 3 shows typical temperature distributions in the flowfield along and perpendicular to the flow axis in the vertical condenser for different heat inputs. Solid lines were derived from data obtained from laser holographic interferograms. Symbols were produced from thermocouples of the A-group along the adiabatic wall (where $Y=0.9$) and from the E-group perpendicular to the cold wall (where $X=1.2$). The origin and the X,Y coordinate system in the figure were those designated in Fig. 1b. A fairly good agreement was reached from the measurement by thermocouples and by laser holographic interferograms. The profiles along the flow axis are usually explained as being typical of a "vapor-gas interfacial layer" in the VCHP and have been treated as such in one-dimensional analyses.[2] However, the two-dimensional profiles shown in this figure (see also photographs in Fig. 5) have been reported infrequently in the literature. A fairly thick condensation boundary layer created on the cooled wall and its effect on heat transfer rate should be investigated more

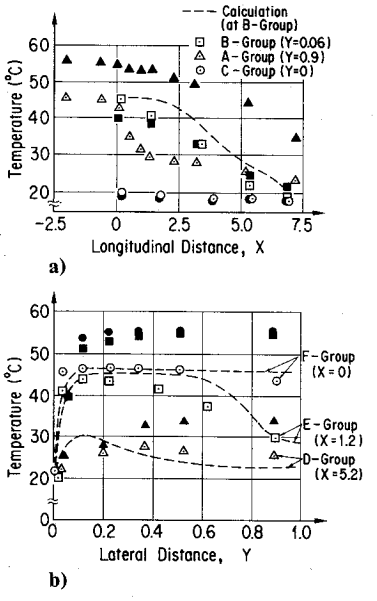

Fig. 4 Temperature distributions along and perpendicular to flow axis in the near-horizontal condenser for bottom-cooled (open symbols) and top-cooled condition ($Q=30.5$ W, $n_G=0.0006$ mole).

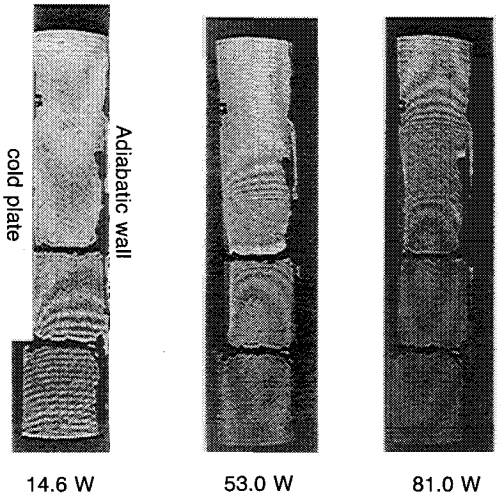

Fig. 5 Laser holograms of density distributions in the flowfield of vertical condenser for different heat load ($n_G = 0.002$ mole).

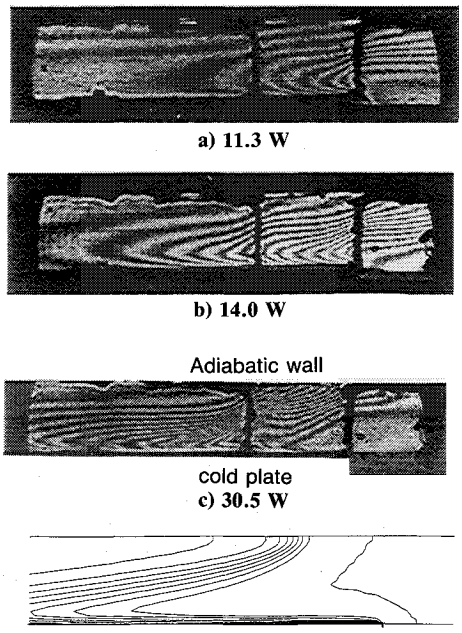

Fig. 6 Laser holograms of density distributions in the flowfield of near-horizontal condenser ($n_G = 0.002$ mole).

Table 1 Typical values for major parameters calculated in the same condition as those of the experiment

Experimental conditions	Calculated parameters	Case 1	Case 2
$n_G(\times 10^{-3}$ mol)		0.6	0.6
Q(W)		26.3	40.6
T_0(°C)		39.6	42.3
T_W(°C)		19.1	20.2
	Re	134.0	204.0
	Pr	0.757	0.755
	Sc	0.423	0.433
	$Gr_T(\Lambda)$	1.48×10^4	1.84×10^4
	$Gr_T(C_V)$	7.08×10^3	8.92×10^3
	$Gr_C(\Lambda)$	-1.04×10^5	-1.26×10^5
	$Gr_C(C_V)$	-5.88×10^4	-7.42×10^4
	Θ_W	14.3	13.3
	N_W	1.65	1.56
	C_{VW}	0.750	0.686
	C_G	0.670	0.583

extensively, as this is critically important in evaluating heat-pipe performance.

Similar temperature distributions measured at different locations of the flowfield in the "near-horizontal condenser" are shown in Fig. 4. The open symbols indicate those for the cold plate positioned on the bottom wall, and the black symbols are those positioned on the top wall. Temperature profiles at positions of the A-group thermocouples are observed to be largely different, depending on the cold plate positions; whereas those at B- and C-group positions are relatively unchanged. The main reason is attributed to the difference of the buoyancy effect, based on the different molecular weights of the vapor and the noncondensable gas.

Typical flow patterns visualized in the vertical condenser and those in the near-horizontal condenser are illustrated in Figs. 5 and 6, from which the temperature distributions are deduced. It should be noted that the fringe patterns of the interferograms obtained in the latter look fairly similar whether the cold plate is located on the top or on the bottom wall (not shown in this paper). Therefore only those of the cold plate positioned on the bottom wall are shown in Fig. 6. The two black shadows across the flowfield and the irregular contour near the adiabatic wall in the figures indicate the shaded area by groups of thermocouples.

Figure 7 shows the average heat transfer rate Nu of the condenser with respect to $RePr$ ($=Pe$, Peclet number) for different n_G conditions. The black symbols, indicating large

Table 2 Comparison of the numerical parameters for benzene and water vapors, mixed with different noncondensable gases

Noncondensable gas	Benzene vapors[a]				Water vapors[b]			
	He	Ne	Air	Ar	He	Ne	Air	Ar
Re	144.0	126.0	134.0	125.0	88.7	60.2	82.1	68.7
Pr	1.69	0.754	0.757	0.724	1.44	0.810	0.867	1.02
Sc	0.111	0.289	0.423	0.474	0.479	0.710	0.701	0.677
$Gr_T(\Lambda)$	1.26×10^4	1.16×10^4	1.48×10^4	1.47×10^4	1.04×10^2	2.38×10^2	7.48×10^2	8.69×10^2
$Gr_T(C_V)$	9.75×10^2	4.16×10^3	7.08×10^3	9.07×10^3	4.77×10^1	2.47×10^2	8.57×10^2	1.07×10^3
$Gr_C(\Lambda)$	-1.57×10^5	-1.03×10^5	-1.04×10^5	-7.50×10^4	-9.28×10^2	1.80×10^2	2.40×10^3	4.73×10^3
$Gr_C(C_V)$	-8.23×10^4	-5.84×10^4	-5.88×10^4	-4.24×10^4	-9.25×10^2	1.47×10^2	1.79×10^3	3.24×10^3
M_W	0.758	1.25	1.65	2.41	0.419	−10.2	−2.81	−1.91
Θ_W	14.3	14.3	14.3	14.3	6.81	6.81	6.81	6.81
C_{VW}	0.750	0.750	0.750	0.750	0.120	0.120	0.120	0.120
C_G	0.670	0.670	0.670	0.670	0.914	0.914	0.914	0.914

[a]Conditions: noncondensable gas = 0.6×10^{-3} mol; heat input = 26.3 W; inlet temp. = 39.6°C; wall temp. = 19.1°C. [b]Conditions: noncondensable gas = 0.8×10^{-3} mol; heat input = 155.0 W; inlet temp. = 55.0°C; wall temp. = 13.0°C.

Nu values, are for condensation of pure vapor ($n_G = 0$). A tendency of decreasing the *Nu* gradient with increasing *Pe* implies the saturation of cooling capability of this apparatus. In the case where $n_G \neq 0$, values of *Nu* are almost linearly proportional to *Pe*, and their gradient decreases with increasing n_G values. This means that Stanton number *St* ($=Nu/Pe$) is approximately inversely proportional to n_G. This trend seems to be typical for the heat transfer phenomena that take place in the VCHP.

Summary of experimental results are as follows: profiles and locations of the vapor-gas interfacial layer produced in the condenser are influenced strongly by the gravity force but weakly by the direction of the vapor condensation, caused mainly by binary diffusion in the present experiment. In other words, formation of the interfacial layer is primarily affected by the molecular weight ratio of the constituents in the condenser. This implies that we should be cautious when discussing diffusion-front models in the condenser of a VCHP. The proposal of an interfacial layer across the flowfield in the condenser may not always be correct for VCHPs under the effect of a gravity force.

Numerical Calculation

Two typical conditions were chosen to compare experimental data with numerical data, as shown in Fig. 8. The conditions and important output parameters which were examined are summarized in Table 1. Temperature distributions at the A-group thermocouple positions were also compared with experimental data in Fig. 4, designated by dotted lines. Both profiles are in fairly good agreement except in the vicinity of the adiabatic wall (B-II) where the Teflon wall may not act as a complete insulator. These results prove that it is valid to apply this analytical model to vapor-flow investigations in the VCHP or thermosyphon.

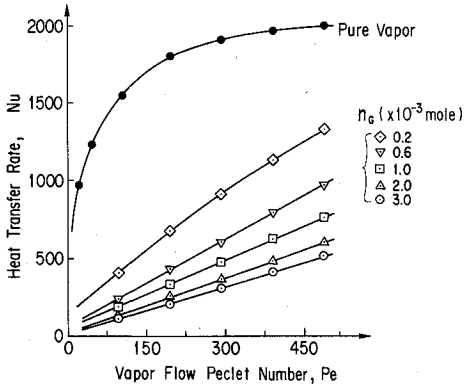

Fig. 7 Heat transfer rate of vertical condenser with respect to flow Reynolds number and noncondensable gas levels.

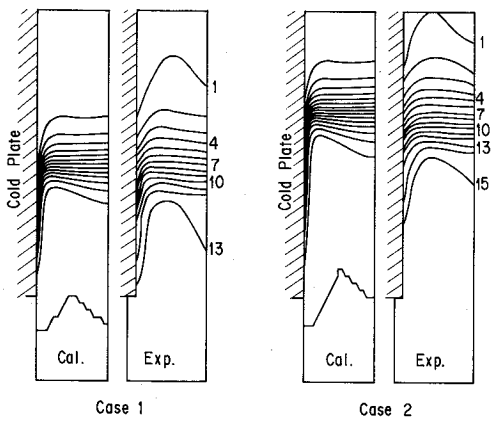

Fig. 8 Comparison of simulated and experimental flowfield for benzene-air mixture for two cases summarized in Table 1.

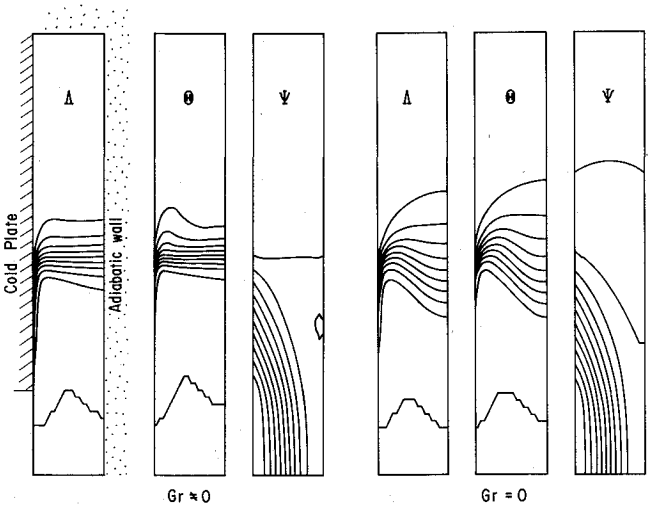

Fig. 9 Comparison of numerical flowfield parameters with and without gravity.

To confirm the further validity of the analysis, the numerical investigation of the flowfield was performed making a parametric study with respect to *A* and *Gr*. The difference of using C_V and Λ for *A* in Eq. (9) on the calculated results is mainly reflected in the two buoyancy terms Gr_C and Gr_T. It was found that, when $M_V > M_G$ (benzene-air mixture), a larger value of *Gr* was obtained by adopting Λ for *A*; whereas in the case of $M_V < M_G$ (water-argon mixture), a larger value of Gr_C was obtained by using C_V. The two experimental conditions were selected to evaluate the numerical parameters the results of which are summarized in Table 2. However, those profiles of *A*, Θ, and ψ obtained for Λ and C_V in Eq. (9) were found to be almost the same, except in the vicinity of the cooled plate where the profiles were closer to the experimental data when using Λ. Further, it was found that the thickness (or axial distance of large density gradient) of the interfacial layer may not change appreciably unless the difference of Gr_C values becomes large enough to be more than an order of magnitude.

The effect of the gravity force on flow profiles is significant, as shown in Fig. 9, where case 1 in Table 1 is illustrated with or without gravity force ($Gr_C = Gr_T = 0$). The temperature field is affected more strongly by the gravity force than the concentration field, and a local region of separated flow appears in the gravity condition. On the contrary, without gravity, the diffusion effect becomes more prominent, resulting in a thicker interfacial layer with no separation bubbles in the flowfield. Dimensionless constants, *Pr* and *Sc* also considerably affect the thickness of the interfacial layers of Θ and *A* in a complicated manner depending on the relative significance of these values with respect to *Gr*. A numerical concentration profile conducted for a near-horizontal condenser under experimental conditions corresponding to those of Fig. 6c is illustrated in Fig. 6d. Both flow profiles agree fairly well, at least qualitatively. It should be remarked that these profiles are quite different from those of the vertical condenser indicating no clear interfacial layers in the flowfield.

Conclusion

A condensing vapor flowfield with large temperature differences between the vapor and the wall surface was investigated experimentally and analytically. Major conclusions obtained from these results are summarized as follows:

1) The profiles and locations of the interfacial layer appearing in the flowfield of a vertical VCHP are strongly dependent on the gravity force. However, the near-horizontal condenser may have no such clear layers in the flowfield

owing to ineffectiveness of the gravity force on the flowfield in suppressing the binary diffusion along the flow axis. This implies that the well-known principle of a one-dimensional, diffusion-front model may not necessarily be applicable to VCHPs for terrestrial use or for a laboratory setup under gravity conditions.

2) The proposed analytical model for vapor flow, associated with vapor-noncondensable gas interactions, successfully explains the feature of the flowfield proving its validity as a tool to investigate a similar vapor flow in the container, although further improvements in the algorithm are still necessary.

References

[1]Cotter, T. P., "Theory of Heat Pipes," Los Alamos Scientific Lab. Albuquerque, NM, Rept. LA-3246-MS, March 1965.

[2]Marcus, B. D., "Theory and Design of Variable Conductance Heat Pipes," NASA CR-2018, 1972.

[3]Sparrow, E. M., and Marschall, E., "Binary, Gravity-Flow Film Condensation," *Journal of Heat Transfer, Transaction of ASME*, May 1969, pp. 205–211.

[4]Rohani, A. R., and Tien, C. L., "Steady Two-Dimensional Heat and Mass Transfer in the Vapor-Gas Region of a Gas-Loaded Heat Pipe," *Journal of Heat Transfer, Transaction of ASME*, Aug. 1973, pp. 377–382.

[5]Krishna, R., and Panchal, C. B., "Condensation of a Binary Vapor Mixture in the Presence of an Inert Gas," *Chemical Engineering and Science*, Vol. 32, No. 7, 1977, pp. 741–745.

[6]Seban, R. A., and Hodgson, J. A., "Laminar Film Condensation in a Tube with Upward Vapor Flow," *International Journal of Heat Mass Transfer*, Vol. 25, No. 9, 1982, pp. 1291–1300.

[7]Kobayashi, Y., and Matsumoto, T., "Vapor Condensation in the Presence of Non-Condensable GAS in the Gravity Assisted Thermosyphon," *Proceedings of 6th International Heat Pipe Conference*, CENG, Grenoble, France, Vol. 2, 1987, pp. 565–570.

[8]Busse, C. A., and Prenger, F. C., "Numerical Analysis of the Vapor Flow in Cylindrical Heat Pipes," *Proceedings of 5th International Heat Pipe Conference*, JATEC, Tokyo, Vol. 1, 1984, pp. 214–219.

[9]Kobayashi, Y., and Matsumoto, T., "Two-Dimensional Condensing Vapor Flow on Parallel Flat Plates in an Enclosure," *Journal of Thermophysics and Heat Transfer*, Vol. 1, No. 2, 1987, pp. 122–128.

[10]France, D. M., Carlson, R. D., and Roy, R. P., "Measurement and Analysis of Dynamic Instabilities in Fluid-Heated Two-Phase Flow," *International Journal of Heat and Mass Transfer*, Vol. 29, No. 12, 1986, pp. 1919–1929.

[11]Lin, Y. S., and Akins, R. G., "Pseudo-Steady-State Natural Convection Heat Transfer Inside a Vertical Cylinder," *Journal of Heat Transfer, Transaction of ASME*, Vol. 108, May 1986, pp. 310–316.

[12]Reed, J. G., and Tien, C. L., "Modeling of the Two-Phase Closed Thermosyphon," *Journal of Heat Transfer, Transaction of ASME* Vol. 109, Aug. 1987, pp. 722–730.

[13]Peterson, P. F., and Tien, C. L., "Gas-Concentration Measurements and Analysis for Gas-Loaded Thermosyphons," *Journal of Heat Transfer, Transaction of ASME*, Vol. 110, June 1988, pp. 743–747.

[14]Bedingfield, C. H., Jr., and Drew, T. B., "Analogy Between Heat Transfer and Mass Transfer—A Psychrometric Study," *Industrial and Engineering Chemistry*, Vol. 42, No. 6, 1950, pp. 1164–1173.